bioRxiv preprint doi: https://doi.org/10.1101/2021.09.06.459178; this version posted September 15, 2021. The copyright holder for this preprint (which was not certified by peer review) is the author/funder. All rights reserved. No reuse allowed without permission.

**Title**: Ecological constraints on highly evolvable olfactory receptor genes and morphology

1

- 3 Authors: Laurel R. Yohe<sup>1,2,3,4\*</sup>, Matteo Fabbri<sup>1,5</sup>, Daniela Lee<sup>1,6</sup>, Kalina T.J. Davies<sup>7</sup>, Thomas P. Yohe<sup>8</sup>, Miluska K.R. Sánchez<sup>9</sup>, Edgardo M. Rengifo<sup>10,11</sup>, Ronald Hall<sup>12</sup>, Gregory Mutumi<sup>12</sup>, Brandon 4 P. Hedrick<sup>13</sup>, Alexa Sadier<sup>14</sup>, Nancy B. Simmons<sup>15</sup>, Karen E. Sears<sup>14</sup>, Elizabeth Dumont<sup>12</sup>, Stephen 5 J. Rossiter<sup>7</sup>, Bhart-Anjan S. Bullar<sup>1,16</sup>\*, Liliana M. Dávalos<sup>2,17</sup>\* 6 7 8 Affiliations: 9 <sup>1</sup>Department of Earth and Planetary Sciences, Yale University, New Haven, CT, USA <sup>2</sup>Department of Ecology and Evolution, Stony Brook University, Stony Brook, NY, USA 10 <sup>3</sup>Deaprtment of Genomics and Bioinformatics, University of North Carolina at Charlotte, 11 12 Charlotte, NC, USA <sup>4</sup>North Carolina Research Campus, Kannapolis, NC, USA 13 <sup>5</sup>Field Museum of Natural History, Chicago, IL, USA 14 15 <sup>6</sup>Harvard School of Medicine, Cambridge, MA, USA 16 <sup>7</sup>School of Biological & Chemical Sciences, Queen Mary University London, London, UK 17 <sup>8</sup>Independent Software Engineer, Centerville, OH, USA <sup>9</sup>Escuela Profesional de Ciencias Biológicas, Universidad Nacional de Piura, Piura, Peru 18 19 <sup>10</sup>Programa de Pós-Graduação Interunidades em Ecologia Aplicada, Escola Superior de Agricultura 'Luiz de Queiroz', Centro de Energia Nuclear na Agricultura, Universidade de São 20 21 Paulo, Piracicaba, Brazil 22 <sup>11</sup>Centro de Investigación Biodiversidad Sostenible (BioS), Lima, Peru
- 23 <sup>12</sup>School of Natural Sciences, University of California, Merced, Merced, CA, USA
- 24 <sup>13</sup>Department of Anatomy and Cell Biology, Louisiana State University Health Sciences Center,
- 25 New Orleans, LA, USA
- 26 <sup>14</sup>Department of Ecology and Evolutionary Biology, UCLA, Los Angeles, CA, USA
- 27 <sup>15</sup>American Museum of Natural History, New York, NY, USA
- 28 <sup>16</sup>Yale Peabody Museum of Natural History, Yale University, New Haven, CT, USA
- 29 <sup>17</sup>Center for Inter-Disciplinary Environmental Research, Stony Brook University, Stony Brook,
- 30 NY, USA
- 31

1 2

# 32 **\*Corresponding Authors**:

- 33 Laurel R. Yohe; Yale University; <u>laurel.yohe@yale.edu</u>; <u>lyohe1@uncc.edu</u>
- 34
- 35 Bhart-Anjan Bhullar; Yale University; <u>bhart-anjan.bhullar@yale.edu</u>
- 36
- 37 Liliana M. Dávalos; Stony Brook University; <u>liliana.davalos@stonybrook.edu</u>
- 38
- 39

# 40 Abstract

41 While evolvability of genes and traits may promote specialization during species diversification, how ecology subsequently restricts such variation remains unclear. 42 Chemosensation requires animals to decipher a complex chemical background to locate 43 44 fitness-related resources, and thus the underlying genomic architecture and morphology must cope with constant exposure to a changing odorant landscape; detecting adaptation amidst 45 46 extensive chemosensory diversity is an open challenge. Phyllostomid bats, an ecologically 47 diverse clade that evolved plant-visiting from an insectivorous ancestor, suggest the evolution of novel food detection mechanisms is a key innovation: phyllostomids behaviorally rely 48 49 strongly on olfaction, while echolocation is supplemental. If this is true, exceptional variation in underlying olfactory genes and phenotypes may have preceded dietary diversification. We 50 51 compared *olfactory receptor (OR)* genes sequenced from olfactory epithelium transcriptomes 52 and olfactory epithelium surface area of bats with differing diets. Surprisingly, although OR 53 evolution rates were quite variable and generally high, they are largely independent of diet. 54 Olfactory epithelial surface area, however, is relatively larger in plant-visiting bats and there is an inverse relationship between OR evolution rates and surface area. Relatively larger 55 56 surface areas suggest greater reliance on olfactory detection and stronger constraint on maintaining an already diverse OR repertoire. Instead of the typical case in which 57 specialization and elaboration is coupled with rapid diversification of associated genes, here 58 59 the relevant genes are already evolving so guickly that increased reliance on smell has led to 60 stabilizing selection, presumably to maintain the ability to consistently discriminate among 61 specific odorants – a potential ecological constraint on sensory evolution.

62

## 63 Significance Statement

The evolutionary relationship between genes and morphology is complex to decipher, and 64 macroevolutionary trends are often measured independently; this is especially challenging to 65 66 quantify in unstable genomic regions or hypervariable traits. Odorant cues are detected by proteins encoded by the largest and fasted-evolving gene family in the mammalian genome 67 and expressed in epithelia distributed on elaborate bony structures in the nose, posing a 68 69 challenge to quantification. Yet, the direct interaction of the olfactory system with 70 environmental signals strongly suggest that selection shapes its immense diversity. In 71 neotropical bats, where reliance on plant-visiting evolved from an insectivorous ancestor, we 72 discovered clear dietary differences amongst species, but only after considering morphological 73 and molecular data simultaneously, emphasizing the power of a coupled analysis.

74

## 75 Introduction

Many cellular pathways are under strong constraint to maintain function: the fixation
of potentially lethal mutations can disrupt core functions, and thus natural selection more
frequently removes than favors novel mutations. However, systems that are more exploratory

79 in nature in that they must interact with an ever-changing environmental space (*e.g.* adaptive immunity, host-detection avoidance (1, 2)) may possess a greater capacity to evolve, *i.e.* 80 increased evolvability. With increased variation, there is more opportunity to generate 81 82 phenotypic diversity and interact with new stimuli, facilitating the occupation of novel 83 adaptive zones (3, 4). At the same time, rampant diversification is expected to come under constraint from ecological limits (5). New variation may enable exploration of novel niche 84 85 space, but once a shift has occurred into a new adaptive zone, selection may fine-tune genes 86 and phenotypes to optimize performance within that environment. As a result, specialization will occur, and novel constraints will maintain that specialized system in the new zone. While 87 88 previous work has demonstrated how increased heritable variation may promote evolvability (1), the evidence for how ecology restricts this disparity is less well understood. 89

90 The mammalian olfactory system offers an excellent framework for evaluating the genomic and phenotypic evolvability with respect to ecological diversity. Here, the genetic and 91 92 morphological components of scent detection are both highly variable and interactive, 93 resulting in a complex environmental chemical space directly relevant to fitness (6). In contrast to host-pathogen immunity and infection dynamics, in which there is an evolutionary drive to 94 95 either infect or avoid infection, the fitness consequences of the vast functional repertoire of 96 the olfactory system may be less dire on average. Olfactory receptor genes (ORs) encode G-97 protein-coupled receptor proteins that combinatorially respond to chemical bouquets, that relay signals critical to finding food, avoiding predators, attracting mates, avoiding noxious 98 99 chemicals, identifying conspecifics, and caring for offspring (7, 8). The OR multigene family is both the largest and among the fastest-evolving protein-coding gene families in the 100 101 mammalian genome (9, 10). The highly evolvable nature in this family extends throughout 102 tetrapods (11). The patterns observed in the OR multigene family are generated via a birth-103 death evolutionary process of tandem gene duplication, leading to highly clustered unstable 104 genomic regions (12). Gene duplication generates new substrates for selectable variation: so 105 long as negative dosage effects are minimal, new gene copies are released from selective 106 constraints and can accumulate novel mutations through which the gene can diversify or lose 107 function (13).

108 At the phenotypic level, OR genes are expressed in a monoallelic manner, such that a 109 single copy of each OR gene is expressed per single olfactory sensory neuron (14-16). These 110 neurons are embedded in olfactory epithelial tissue and distributed throughout the 111 posterodorsal region of the nasal cavity, along with glandular supporting cells that facilitate 112 odorant deposition (17). Receptors bind to chemical ligands in a combinatorial fashion (18), 113 depolarize the cell, and send converging signals to be interpreted in the olfactory bulb (19). 114 The olfactory epithelium covers turbinal bones (turbinates), delicate, scroll-like arrangements 115 of approximately five bones, whose shapes can change the surface area for potential odorant 116 deposition. Olfactory turbinals are highly convoluted and variable in shape (20-23), but micro-117 computed tomography (µCT) scanning and image analysis now makes large-scale comparative

118 analyses of these complex structures are now tractable (24). Evidence for selection shaping 119 the size, shape, and relative orientations of turbinates is emerging, including convergent 120 expansion of turbinates in worm-feeding rodents (25) and convergent signatures of tradeoffs 121 of olfactory and respiratory turbinates in amphibious rodents (26). The extensive variation of 122 olfactory turbinates may be in some way coupled with the variation within the OR gene family. 123 Though such a connection has never been explicitly tested, expansion of olfactory turbinates 124 may expand OR expression. The established connection of olfactory turbinates and divergent 125 ecologies (25, 26) offers the opportunity to explore a relationship among evolvability of OR 126 genes, olfactory morphology, and ecological constraints.

127 We investigate evolutionary patterns in OR genes and turbinates in > 30 bat species 128 (Fig. 1; Fig. S1; Table S1, S2) representing the ecologically diverse clade of neotropical leaf-nosed 129 bats (Phyllostomidae) and their close relatives within the superfamily Noctilionoidea. 130 Noctilionoid bats show exceptional diversity in food resource consumption, occupying perhaps 131 the widest arrange of dietary niches of any clade of mammals (27). While most echolocating 132 bats are insectivorous, noctilionoids have diversified to specialize on arthropods, small vertebrates (*e.g.*, fishes, frogs, birds), blood, fruit, pollen, and nectar. A suite of morphological 133 134 and sensory traits is associated with divergent dietary consumption (27, 28). In concert with these changes, bats that feed on anything other than arthropods must evolve novel sensory 135 136 mechanisms for finding new foods (29). The unstable and duplicative nature of OR genes as 137 well as the highly variable features of olfactory turbinates may provide a pool of selectable 138 variation to enable a shift into novel niches. If adaptive selection and/or novel morphologies 139 occurred in the olfactory system prior to the evolution of consuming plant resources, then rates of evolution in ORs should be higher, ORs should have greater allelic diversity to 140 141 potentially detect novel plant compounds, and/or divergent phenotypic optima should be 142 observed in plant-visiting versus animal-feeding bats. Alternatively, though not mutually 143 exclusive, the extensive variation may be constrained by novel dietary niches to optimize or 144 fine-tune specific detection. We explore two scenarios: [1] the molecular and morphological 145 basis of olfaction facilitated the ecological breakthrough of plant consumption, or [2] the 146 constraints of finding specific plants restricted the diversity of the hypervariable olfactory 147 system. We compared sequence variation from expressed ORs from olfactory epithelium 148 transcriptomes to the surface area of olfactory epithelia from high-resolution soft tissue  $\mu$ CT-149 scans of over 30 species with divergent diets. This is among the first datasets of its kind, 150 enabling us to test how ecological variation in diets might shape the evolutionary dynamics 151 of olfactory evolvability

152

## 153 Results

154 To study the variation of the olfactory system at both the morphological and molecular levels,

- we compared surface area of the main olfactory epithelium (n = 30) and used RNA-seq (n = 30)
- 156 of the main olfactory epithelium to sequence *OR*s in species with divergent diets, of which 18

species had both morphological and molecular data. Species were coded either as animalfeeding (n = 15) or plant-visiting (n = 26), based on published ecological metrics (Fig. S1; n = 30).

160

# 161 *Exceptional variation in gross turbinate morphology throughout Yangochiroptera*

162 To test whether plant-visiting bats had more olfactory epithelia relative to animal-feeding, we 163 measured the surface area of the olfactory epithelium distributed in the nasal cavity from µCT-164 scans of iodine-stained specimens collected from 30 species with divergent diets (Fig. S1, Table S1). Despite extensive variation, plant-visiting bats consistently had gualitatively more well-165 166 developed olfactory epithelia (Fig. 2A), though this relationship is statistically complex as described below. Within Phyllostomidae, as well as most other previously studied-members of 167 168 the suborder Yangochiroptera, there are normally five turbinate bones in which the main 169 olfactory epithelium is distributed in the nasal cavity(24, 31, 32). From anterior to posterior 170 with corresponding segmented colors (Fig. 2A), these include the frontoturbinal (pink), 171 ethmoturbinal I (teal), interturbinal II (potentially homologous with ethmoturbinal I (pars 172 posterior) (33); orange), ethmoturbinal II (green), and ethmoturbinal III (purple). Residual main 173 olfactory epithelium (yellow) can also be observed on medial parts of the nasal septum and 174 superior portions of the nasal cavity and olfactory recess. A concern for detecting true olfactory 175 epithelial tissue versus respiratory epithelium is warranted in bats, as the two epithelia can 176 coexist on some turbinals. However, while precise boundaries can only be determined with 177 histology, the two can be distinguished in the diceCT scans (Fig. 2B), in which olfactory 178 epithelium is thick, bright, and smooth while respiratory epithelium is more uneven with bright 179 glandular globules distributed throughout. Most specimens possessed the five described 180 olfactory turbinate bones (Fig. 1), though the structures of each turbinate were highly variable. A sixth turbinal was present in two species; in *Brachyphylla pumila*, a second interturbinal 181 182 (described as interturbinal I in Yohe et al. (2018)) containing dense olfactory epithelia was 183 present between the frontoturbinal and ethmoturbinal I; and in *Desmodus rotundus*, an extra 184 anterior turbinate bone with olfactory epithelia was observed, which we name frontoturbinal 185 0 to avoid confusion with the common notation of frontoturbinal for the standard most 186 anterior turbinate bone. *Myotis albescens* and *Molossus rufus* were missing interturbinal I, but 187 a small extra olfactory-epithelium-bearing turbinal was present in the posterior-most region 188 of the olfactory recess. This extra turbinal was not present in the congeneric *Molossus* 189 molossus.

190

191 *Robust evidence for allometry, weak evidence of selection in olfactory epithelium surface area* 

To first control for body size and explore how it may relate to diversity in olfactory epithelium
surface area, we explored several comparative methods to quantify this relationship.
Evolutionary allometric models tend to assume a single intercept and slope explains the

195 relationship of a given trait to log mass, but adaption yields different intercepts, and the

allometric slope may not be uniform across clades. We used body mass (q) measured directly 196 197 from the live specimen in the field as the proxy for size. Analyses of directional evolution of 198 surface area as a function of body mass identified a multi-optima, single slope model as the 199 one with the highest marginal likelihood (-30.8) compared to others (<-45.8). Posterior 200 parameter estimates summarized in Table S3, however, show weak support for multiple optima 201 and estimates of the directional evolution parameter alpha were lower than the random walk 202 parameter  $\sigma^2$ . Inspection of the posterior probabilities for change in optima in the phylogeny 203 revealed a >0.50 probability in the ancestor of mormoopids (Fig. S2), four optima with a >0.25204 probability (Fig. 2C) and shifts in eleven branches with a posterior probability >0.1 (Fig. 2D). In 205 the scenario with many optima (mean = 6; lower = 1, upper = 12) and corresponding shifts from 206 one optimum to another, shifts are distributed across the tree and unrelated to plant-eating. 207 There was no statistically significant separation by diet.

208

209 When testing whether olfactory epithelial surface area was different in plant- and animal-210 feeding bats, analyses of allometric scaling using phylogenetic regressions found a model with 211 different intercepts and slopes by plant-feeding to best fit the data (DIC: 52.6 versus DIC > 53 212 for simpler models (i.e., single slope/intercept)), suggesting differences amongst the two 213 groups. Without the mormoopids (Fig. 2E), posterior estimates of the allometric slope 214 overlapped with those obtained using directional models (mean slope = 0.39, lower = 0.04, 215 upper = 0.75). There was a trend toward higher slopes for plant-eating species (mean slope = 216 0.094, lower = 0.089, upper = 0.47) compared to animal-eating ones (mean slope = -0.098, lower 217 = -0.46, upper= -0.93; Fig. 2C). Including all taxa, results were similar, except posterior estimates 218 of the allometric slope were higher (mean slope = 0.47, lower = 0.11, upper = 0.93; Fig. S3).

219

220 OR codon evolution explained by OR subfamily and nucleotide substitutions, not ecology

Plant-visiting bats may require a diverse or faster-evolving repertoire of olfactory repertoire since they rely on complex plant volatile bouquets for their food detection, and we tested this hypothesis by sequencing the transcriptomes of the main olfactory epithelium, identifying intact olfactory receptor genes, and comparing amongst plant- and animals-feeders. Highcoverage RNA-seq data (Fig. S1; Table S4, S5) was obtained and intact olfactory receptors were identified and classified into their respective subfamilies. Of the 30 species, an average of 221

(±95) ORs were detected, with large variation among species (Fig. S1; Table S6). Mormoops
 blainvillei had only one intact reading frame and, due to low detection, was removed from

- downstream analyses. There was a weak positive relationship (slope =  $0.004 \pm 0.002$ ;  $F_{(1,28)} = 4.6$ ;
- 230 p = 0.041) between number of *OR*s detected and RNA Integrity Number (RIN; Fig. S4). Because
- previous study found that transcriptomes of the main olfactory epithelium only recover 50-
- 232 60% of total intact *OR* genes (34). Thus, in addition to high rates of duplication and low rates
- of homology among *OR*s, incomplete RNA-seq data may confound comparisons of numbers of receptors across species. Instead, we measured rates of evolution for each gene per species.

#### 235

236 To measure differences in rates of evolution between animal-feeding and plant-visiting bats, 237 we used cumulative root-to-tip branch lengths for several reasons. First, comparing codon and 238 nucleotide rates from their corresponding trees is conceptually similar to measures of 239 molecular selection such as ratios of rates of nonsynonymous substitutions (dN) to rates of synonymous substitution (dS) (11). Second, this method has the added advantage of 240 241 incorporating both codon and different nucleotide substitution models into the best-fit 242 models, incorporating additional information such as transition and transversion parameters 243 when appropriate to the data set. In this case, codon models were used instead of amino acid 244 substitution models, as the former were better fits for all olfactory receptor subfamilies. Third, and crucially, the branch length approach helps overcome the issue of determining true 245 246 orthology versus paralogy, which is very challenging in large gene families. Resulting branch 247 lengths in nucleotide substitutions per codon site for codon-based trees and nucleotide 248 substitutions per site for nucleotide trees are directly comparable across the entire phylogeny. 249 The best-fit model of codon lengths as a function of nucleotide lengths including mormoopids 250 partitioned both intercepts and slopes by gene subfamily (DIC: -18085; Fig. 3). There was no 251 support for partitioning intercepts or slopes by plant diet, diet categories, or species (DIC > -252 11433; Fig. 3A). With the best-fit model, we detected a higher slope in the codon rate for OR 253 subfamily 52, and lower slope for subfamilies 11 and 2/13 (Figs. 3B and 3E). The resulting model 254 captured important differences in rate scaling across gene subfamilies, as shown in 255 comparisons between observed and predicted values (Fig. S5). The PCA found 96.1% of the 256 variation was loaded in the first principal component, with most of the variation explained by 257 the codon branch lengths. When visualizing clusters within the PCA axes, there was no 258 clustering by diet (Fig. 2C) but clear clustering of different *OR* subfamilies.

259

260 Inverse relationship between OR evolution and olfactory epithelium surface area

- 261 Finally, we tested whether there was a molecular-morphological relationship that may explain 262 differences in diet. In multi-response models, both codon branch lengths and olfactory 263 epithelium surface area are responses with their own modeled errors. Thus, the estimated 264 coefficients must be interpreted in a multivariate framework. The best multi-response model 265 including mormoopids (DIC: -37342) only had a weak trend for log body mass of plant-eating 266 bats relating to codon rates (mean slope = -0.0038, lower = -0.0128, upper = 0.0042, Fig. 4; Fig. 267 S6, including mormoopids). In contrast, when excluding mormoopids, the best multi-response 268 model (DIC: -35451) found a strong inverse relationship between codon rates (mean slope: -269 0.034, lower = -0.042, -0.028; Fig. 4A) and olfactory epithelium surface area (slope: -1.36, lower 270 = -1.62, upper = -1.12; Fig. 4B). After accounting for phylogeny, codon lengths, and body mass, 271 the coefficients of body mass on olfactory epithelium surface area for both animal-feeding 272 (mean = 0.38, lower = -0.012, upper = 0.79) and plant-visiting bats are positive, but substantially
- higher for plant-visiting bats (Fig. 4; mean = 0.68, lower = 0.23, upper 0.65).

## 275 Discussion

276 Highly evolvable genes and phenotypes are often associated with exploratory systems, for 277 which variation does not come at the same potential fitness cost as they do for central core 278 processes (5). Yet, when novel variable mutants are favored in a given niche, environmental 279 conditions may subsequently constrain that variation to maintain those variants(5). While 280 previous emphasis has been on the unstable genomic architecture (i.e., arrangement of 281 functional elements(35)) underlying highly evolvable genes and traits, the operation of 282 environmental constraints on this variation is less understood. Using the highly evolvable 283 olfactory system in a clade of bats with divergent dietary ecologies, we have discovered that, although there is exceptional variation in both olfactory morphology (Fig. 2) and OR genes (Fig. 284 285 3), bats that use plant resources show an inverse relationship between rates of molecular and 286 morphological evolution (Fig. 4). Having hypothesized a single expansion or shift to facilitate 287 plant-visiting, we expected strong association of molecular rates and morphological 288 differences with plant-visiting (*i.e.*, Fig. 2C, 2D would show clear shifts with plant association; 289 Fig. 3A, 3C would have ecological signatures;). Instead, we found shorter OR molecular branch 290 lengths in bats with larger epithelial surface area, despite ubiquitous elevated rates of 291 molecular and morphological evolution. We propose that once bats evolved plant-visiting, the 292 exploratory background of a rapidly evolving olfactory system was suddenly exposed to strong 293 selection for maintenance of the ability to detect specific plant odorants any may even enabled 294 convergent plant-visiting to evolve within *Phyllostomus*. This "slowdown" could be important 295 for fine-tuning associations with plants to optimize for detecting fruit ripeness, floral blooms, 296 and/or avoiding toxicity.

297 Without considering morphology, a strong association between evolutionary codon-to-298 nucleotide rate with OR subfamily (Fig. 3B, 3D, 3E) suggests most of the variation in OR is 299 endogenous, instead of ecological (Fig. 3A, 3C); some subfamilies (*e.g.*, OR52, OR4) are evolving 300 at faster rates than others. Within genomes, loci within OR subfamilies tend to be highly 301 clustered, and in bats, many times the entire OR subfamily was detected within a single 302 scaffold(34). This highly-clustered nature is caused by rampant tandem duplication (36), which 303 contributes to the unstable genomic architecture of the system. We hypothesize this instability 304 is the genetic mechanism that generates exceptional variation in chemosensory genes, and 305 that OR genes (and likely other chemosensory receptor genes) are not as constrained as most 306 protein-coding genes (37). Most OR proteins are highly specific and are not involved in core 307 cellular pathways (*i.e.*, they have minimal pleiotropy) (37). Their main function is to initiate G-308 protein coupled receptor pathway responses and to "survey" and respond to environmental 309 chemical cues (*i.e.*, they are, as pathogen-detection, proteins exploratory proteins). Thus, we 310 predict that duplication of OR genes does not have strong dosage effects. Instead, duplication 311 might increase the probability of expression for a given receptor or increase the genomic 312 substrate for new mutations to arise. Indeed, it is the standing variation within these

313 contingency loci that contributes to the "adaptability" of chemosensory receptor genes in314 divergent *Drosophila* populations (37).

315 The genetic controls of olfactory turbinate morphogenesis are unrelated to OR genes 316 (but rather more so the olfactory bulb) (38), but the expansion of olfactory epithelium surface 317 area directly increases the neural epithelial space in which olfactory receptor neurons can 318 express OR genes. While the expression of OR genes is monoallelic and stochastic per sensory 319 neuron (14–16), there is zonal organization of expression within the turbinates associated with 320 different OR subfamilies. This zonation is complex in 3D space. OR gene subfamilies are not 321 distributed on specific turbinates, but instead spatially distributed across turbinates in 322 space(39). The more outward parts of the turbinates express similar receptor families 323 compared to zones closer to the olfactory bulb(40). Although further research both establishing 324 the boundaries of these zones and the functional differences among *OR* subfamilies regarding 325 odorant molecule binding is necessary to properly interpret differences in relation to 326 evolutionary niche divergence, our study identifies a key relationship between morphology and 327 OR gene repertoire. Modeling errors in both morphology and genes simultaneously (while also 328 accounting for allometry, and phylogeny) in a Bayesian hierarchical framework revealed strong 329 and inverse relationships between protein coding evolutionary rates and surface area among 330 both plant-visiting and animal-feeding bats, with a stronger body mass allometry in the former 331 (Fig. 4). This corroborates our hypothesis that chemosensory system evolution is confounded 332 by high variation that must be accounted for when deciphering evolutionary patterns.

333 It has been previously hypothesized that olfactory key innovations enabled (and 334 continue to enable) the detection of new plant compounds(41). Based on our results, we now 335 hypothesize that standing variation in highly evolvable OR genes and morphology is fine-tuned 336 in plant-visiting phyllostomid bats. Complex interplay of hypervariable morphology (Fig. 2) and 337 receptor repertoire (Fig. 3) may have been ideal for exploring novel niches. However, once shifts 338 into more specialized adaptive zones occurred, selection prevented further extensive change 339 of ORs perhaps to maintain a repertoire that can recognize a diverse but consistent mix of 340 odorant cues. Expanded olfactory epithelial surface area may enable more expression of these 341 conserved, more slowly evolving receptors (Fig. 4).

342 Within the phyllostomid radiation and its close relatives, patterns beyond olfaction 343 support this hypothesis. For morphology, the shift from an insectivorous ancestor to a derived plant specialist is supported by transitional fossils (*i.e.*, omnivorous ancestors) (42), even early 344 345 within the superfamily radiation (e.g., *†Vulcanops jennyworthyae*, an omnivorous burrower (43)). Most craniofacial variation occurs late in development, suggesting the palate and nasal 346 347 cavity regions have fewer constraints and could facilitate morphological evolvability (44). 348 Major transitions in sensory traits occurred early in the radiation, while mechanical feeding 349 shifts were more recent (29). At the molecular level, positive selection in vision and diet related genes occurred mostly at the origins of Phyllostomidae and their relatives, instead of at nodes 350 of dietary shifts towards plant-visiting (45, 46). Thus, a "backbone" of extensive variation linked 351

to omnivory may have set the stage for later shifts to highly specialized diets. In either case, an inverse relationship between morphology and protein-coding evolutionary rate emerged only after controlling for extensive sources of intrinsic variation within the system. This intriguing pattern warrants further investigation of the interplay among *OR* expression, the distribution of the tissue expressing these genes, and how evolution shapes both and their interaction.

358

## 359 Methods

Sample Collection: Specimens for both genetic and morphological analyses were collected over 360 361 the course of five field expeditions: two to the Dominican Republic in 2014 and 2015 (collection permit VAPB-01436), one to Belize in 2014 (Belize Forestry Department Scientific Research and 362 363 Collecting Permit CD/60/3/14), one to Peru in 2015 (collection permit 0002287), and one to Costa 364 Rica in 2017 (collection permit R-041-2017-OT-CONAGEBIO). All genetic tissue and morphological specimens were exported in accordance with research permit and country guidelines. Samples 365 366 were imported in accordance with U.S. Center for Disease Control and U.S. Fish & Wildlife quidelines. All specimens were collected, handled, and euthanized in accordance with Stony 367 368 Brook University IACUC permit 614763-3 for Peru, and 448712-3 for Costa Rica, and Brown 369 University IACUC 1205016 and 1504000134, University of Georgia IACUC AUP A2009-10003-0 and 370 A2014 04-016-Y3-A5 for Belize.

371

372 We sampled sets of diverse species to obtain RNA-seq and morphological data. For tissue 373 collection for RNA-seq, specimens we used published video dissection protocols to sample the 374 olfactory epithelium(47, 48). In total, 30 species were collected for transcriptomic analyses, 375 including one emballonurid, one molossid, two mormoopids, and 26 phyllostomids to represent 376 a diversity of divergent diets (Fig. 1; Fig. S1; Table S1). For morphological sampling, specimens 377 were collected on the same expeditions listed above, and many of the species replicate the 378 samples taken for transcriptomic analyses (Table S2). Body mass was measured from living 379 bats to serve as a proxy for body size. A total 30 species were sampled for morphology, and of 380 these, 19 species had replicates for both genetic and morphological sampling. Both procedures 381 are described in detail in the Supplementary Methods.

382

*Transcriptomics*: RNA extraction and RNA-seq protocols were the same as those described in a previously published study(34). Although there was variation in the cDNA library preparation and RNA sequencing over the course of the project, read lengths only varied from 90bp to 150bp. This variation likely contributes to some differences in transcript assemblies across samples. While the Supplementary Methods describe the full details of RNA-seq, Table S3 shows which sequencing platforms, sequencing company, and read lengths were performed for each sample.

391 *Transcriptome assembly*. Raw reads were trimmed, cleaned, and assembled in accordance with 392 a previously published method (34). In summary, because of the duplicative nature of olfactory 393 receptors, we implemented the Oyster River Protocol v. 2.1.0 (49), which uses three separate 394 assembly programs, pools assembled reads across approaches, and removes duplicate contigs. 395 The Oyster River Protocol also provides several quantifiable measures of assembly quality, 396 including TransRate scores (50) that quantify coverage and segmentation of each transcript.

397

398 Olfactory receptor classification: The assembled transcripts for each species were run through 399 the published program Olfactory Receptor Assigner (ORA) v. 1.9.1(51). The ORA is a Bioperl v. 400 1.006924 program that implements the HMMR v. 3.1b algorithm to characterize olfactory 401 receptors into their respective subfamilies based on conserved binding motifs calculated by 402 the trainer protein alignments. While some pseudogenes were present in the transcriptomes, 403 we limited analyses to intact genes that had the potential to be under diversifying or positive 404 selection.

405

*Quantifying molecular evolution*: Cumulative root-to-tip branch lengths for each tip of the
 codon model and nucleotide model gene trees were performed by computing the variance
 covariance matrix of each tree and extracting the diagonals of this matrix using ape v. 5.4.1(52)
 in R.

410

411 *µCT-scanning and turbinate segmentation*: Formalin-fixed museum specimesn were stained in 412 10% Lugol's iodine solution, mounted in agarose, and scanned in the high-resolution Nikon 413 H225 ST  $\mu$ CT-scanner. Scan parameters varied depending on specimen size and morphology, 414 but resolution voxel size ranged from 0.01 to 0.02 mm per scan. Scan parameter details are 415 available in Table S4. Raw  $\mu$ CT-scan data was reconstructed using in-house Nikon software to 416 align the center of rotation and correct artifacts with beam hardening parameters. 417 Reconstructed image stacks were imported into VGStudio v. 3.3(53). for image segmentation of 418 the main olfactory epithelium. When visible, the olfactory epithelium was segmented using 419 the "magic wand" tool in the right nasal cavity on each observed turbinal and surrounding 420 structures. Each segmented object was smoothed through "closing" each surface by a value of 421 1 and "eroded" by a value of -0.5. Surface areas were calculated within VGStudio after creating 422 a region of interest of the segmented object and estimating its surface determination by 423 setting the isovalue to completely include all segmented values (*i.e.*, the entire histogram).

424

425 Statistical analyses of evolutionary rates: Molecular evolution, specimen collections, and µCT426 scanning yielded three types of data, in order: codon and nucleotide branch lengths, body mass,
427 and olfactory epithelium surface area. Our goal is to integrate molecular evolutionary rates

428 with morphological variation, but first we had to evaluate each data set separately. We

429 therefore implemented three sets of interrelated analyses: 1) regressions and principal

430 components analyses of codon rates as a function of nucleotide rates for each gene, 2)431 phylogenetic regressions of the allometry between olfactory epithelium surface area and body

- 432 mass both with and without accounting for directional selection and varying adaptive peaks,
- 433 and 3) after determining which of the two model types was better supported for anatomical
- 434 data, multivariate analyses of codon and nucleotide branch lengths together with olfactory
- 435 epithelium surface area, with mass as an independent variable.
- 436
- For the first set of regressions, we modeled codon branch lengths as a function of nucleotide lengths. Although all models included nucleotide lengths as an independent variable, we tested for different intercepts and slopes partitioned by plant diet, multiple diet categories, gene subfamily, or species. Details on the error structure used for these groups are presented in the supplement. To evaluate any patterns of separation in the data not captured by the regression models, we also performed a principal components analysis of the codon and nucleotide branch lengths using the prcomp function in R.
- 444
- For the second set of models, we regressed the olfactory epithelium surface area against body
  mass, both in the log scale to determine the evolutionary allometry of the nose anatomy. First,
  we evaluated whether models with directional selection and distinct evolutionary optima were
- 448 appropriate for these data, and then tested a series of phylogenetic regressions with identical
- 449 or differing intercepts, slopes, or both by diet categories. While we used the marginal
- 450 likelihood and parameter estimates to evaluate the directional models, we used the deviance
- 451 information criterion (DIC), to assess the phylogenetic regressions. Details on both directional
- 452 and non-directional allometric are presented in the supplement.
- 453
- In the third suite of models, we related *OR* evolution and olfactory epithelium surface area by implementing multivariate models, allowing both codon branch lengths and surface to be modeled with error. Nucleotide branch lengths and (log) body mass were both included as predictors in these phylogenetic models, with group specific effects outlined in the supplement. The DIC was used to select best-fit models. Finally, all MCMCglmm models ran with and without mormoopid taxa (n=3), as their skull morphology is hypervariable and may confound underlying patterns within the data (28).
- 461

# 462 Acknowledgements

Thank you to Brandon Mercado and the Yale core facilities that support the μCT-scanner. Thank
you to Jesus Almonte and Grupo Jaragua for field assistance in the Dominican Republic. Thank
you to Fanny Cornejo, Carlos Eduardo Tello Chenin, Jorge Carrera, Jaime Pacheco Castillo, Jorge
Ruíz Leveau, and Harold Portocarrero Zarria for field assistance in Peru. This study was
supported by the American Society of Mammalogists to LRY, The Explorer's Club to LRY, Society
for the Study of Evolution Rosemary Grant to LRY, NSF Graduate Research Fellowship to LRY,

- 469 NSF-DEB 1701414 to LRY and LMD, NSF-PRFB 1812035 Postdoctoral Fellowship in Biology to LRY,
- 470 NSF-IOS 2032073 to LRY and BASB, NSF-DEB 1838273 to LMD, NSF-DEB 1442142 to LMD and SJR;
- 471 NSF-DEB 1442314 to KES; and NSF-DEB 1442278 to ERD, the European Research Council (ERC
- 472 Starting grant 310482 [EVOGENO]) awarded to SJR, LSI ECR bridging fund to KTJD. The Indiana
- 473 University Carbonate server funded by NSF-DBI 1458641, the CIPRES Science Gateway (54), the
- 474 SeaWulf computing system from Stony Brook Research Computing and Cyberinfrastructure,
- 475 and the Institute for Advanced Computational Science at Stony Brook University funded by
- 476 NSF-OAC 1531492 provided necessary computational resources for this project. Fieldwork to
- 477 collect Belize samples was supported by the AMNH Taxonomic Mammalogy Fund.

478	References		
479	1.	C. J. Graves, V. I. D. Ros, B. Stevenson, P. D. Sniegowski, D. Brisson, Natural selection	
480		promotes antigenic evolvability. <i>PLoS Pathog.</i> <b>9</b> , e1003766 (2013).	
481	2.	C. N. Merrikh, H. Merrikh, Gene inversion potentiates bacterial evolvability and	
482		virulence. <i>Nat. Commun.</i> <b>9</b> (2018).	
483	3.	N. Feiner, M. Brun-Usan, T. Uller, Evolvability and evolutionary rescue. <i>Evol. Dev.</i> , 1–12	
484		(2021).	
485	4.	G. G. Simpson, <i>The Major Features of Evolution</i> (Simon and Schuster, 1953).	
486	5.	M. Kirschner, J. Gerhart, Evolvability. <i>Proc. Natl. Acad. Sci. U. S. A.</i> <b>95</b> , 8420–8427 (1998).	
487	6.	L. R. Yohe, P. Brand, Evolutionary ecology of chemosensation and its role in sensory	
488		drive. <i>Curr. Zool.</i> <b>64</b> , 525–533 (2018).	
489	7.	S. M. Kurian, et al., Odor coding in the mammalian olfactory epithelium. Cell Tissue Res.	
490		<b>383</b> , 445–456 (2021).	
491	8.	R. L. Doty, Odour-guided behaviour in mammals. <i>Experientia</i> <b>42</b> , 257–271 (1986).	
492	9.	Y. Niimura, A. Matsui, K. Touhara, Extreme expansion of the olfactory receptor gene	
493		repertoire in African elephants and evolutionary dynamics of orthologous gene groups	
494		in 13 placental mammals. <i>Genome Res.</i> <b>24</b> , 1485–1496 (2014).	
495	10.	Y. Niimura, Olfactory receptor multigene family in vertebrates: from the viewpoint of	
496		evolutionary genomics. <i>Curr. Genomics</i> <b>13</b> , 103–14 (2012).	
497	11.	L. R. Yohe, M. Fabbri, M. Hanson, BA. S. Bhullar, Olfactory receptor gene evolution is	
498		unusually rapid across Tetrapoda and outpaces chemosensory phenotypic change. Curr.	
499		<i>Zool.</i> <b>66</b> , 505–514 (2020).	
500	12.	M. Nei, A. P. Rooney, Concerted and birth-and-death evolution of multigene families.	
501		<i>Annu. Rev. Genet.</i> <b>39</b> , 121–152 (2005).	
502	13.	L. R. Yohe, L. Liu, L. M. Dávalos, D. A. Liberles, "Protocols for the molecular evolutionary	
503		analysis of membrane protein gene duplicates" in Computational Methods in Protein	
504		<i>Evolution</i> , T. Sikosek, Ed. (Springer New York, 2019), pp. 49–62.	
505	14.	K. Monahan, S. Lomvardas, Monoallelic expression of olfactory receptors. Annu. Rev.	
506		<i>Cell Dev. Biol.</i> <b>31</b> , 721–740 (2015).	
507	15.	I. Rodriguez, Singular expression of olfactory receptor genes. <i>Cell</i> <b>155</b> , 274–7 (2013).	
508	16.	I. Abdus-Saboor, et al., An expression refinement process ensures singular odorant	
509		receptor gene choice. <i>Curr. Biol.</i> <b>26</b> , 1083–1090 (2016).	
510	17.	F. Liang, Sustentacular cell enwrapment of olfactory receptor neuronal dendrites: An	
511		update. <i>Genes (Basel).</i> <b>11</b> , 14–17 (2020).	
512	18.	S. M. Kurian, <i>et al.</i> , Odor coding in the mammalian olfactory epithelium. <i>PsyArXiv</i> , 1–14	
513		(2020).	
514	19.	DJ. Zou, A. Chesler, S. Firestein, How the olfactory bulb got its glomeruli: a just so	
515		story? <i>Nat. Rev. Neurosci.</i> <b>10</b> , 611–618 (2009).	
516	20.	I. K. Lundeen, E. C. Kirk, Internal nasal morphology of the Eocene primate <i>Rooneyia</i>	

517		<i>viejaensis</i> and extant Euarchonta: Using $\mu$ CT scan data to understand and infer
518		patterns of nasal fossa evolution in primates. <i>J. Hum. Evol.</i> <b>132</b> , 137–173 (2019).
519	21.	I. Ruf, Comparative anatomy and systematic implications of the turbinal skeleton in
520		Lagomorpha (Mammalia). <i>Anat. Rec.</i> <b>297</b> , 2031–2046 (2014).
521	22.	A. A. Curtis, N. B. Simmons, Unique turbinal morphology in horseshoe bats (Chiroptera:
522		Rhinolophidae). Anat. Rec. 00 (2016).
523	23.	B. van Valkenburgh, <i>et al.</i> , Respiratory and olfactory turbinals in feliform and caniform
524		carnivorans: The influence of snout length. Anat. Rec. <b>297</b> , 2065–2079 (2014).
525	24.	L. R. Yohe, S. Hoffmann, A. Curtis, Vomeronasal and olfactory structures in bats
526		revealed by diceCT clarify genetic evidence of function. <i>Front. Neuroanat.</i> <b>12</b> , 1–13
527		(2018).
528	25.	Q. Martinez, <i>et al.</i> , Convergent evolution of an extreme dietary specialisation, the
529		olfactory system of worm-eating rodents. <i>Sci. Rep.</i> <b>8</b> , 1–13 (2018).
530	26.	Q. Martinez, et al., Convergent evolution of olfactory and thermoregulatory capacities
531		in small amphibious mammals. <i>Proc. Natl. Acad. Sci.</i> <b>117</b> (2020).
532	27.	E. R. Dumont, et al., Morphological innovation, diversification and invasion of a new
533		adaptive zone. <i>Proc. R. Soc. B Biol. Sci.</i> <b>279</b> , 1797-1805 (2012).
534	28.	B. P. Hedrick, et al., Morphological diversification under high integration in a hyper
535		diverse mammal clade. <i>J. Mamm. Evol.</i> <b>27</b> , 563–575 (2020).
536	29.	R. P. Hall, et al., Find the food first: An omnivorous sensory morphotype predates
537		biomechanical specialization for plant based diets in phyllostomid bats. Evolution (N.
538		<i>Y).</i> , 1–11 (2021).
539	30.	D. Rojas, M. J. Pereira, C. Fonseca, L. M. Davalos, Eating down the food chain:
540		generalism is not an evolutionary dead end for herbivores. <i>Ecol. Lett.</i> <b>21</b> , 402–410
541		(2018).
542	31.	K. P. Bhatnagar, F. C. Kallen, Morphology of the nasal cavities and associated structures
543		in <i>Artibeus jamaicensis</i> and <i>Myotis lucifugus</i> . <i>Am. J. Anat</i> . <b>139</b> , 167–189 (1974).
544	32.	K. P. Bhatnagar, F. C. Kallen, Quantitative observations on the nasal epithelia and
545		olfactory innervation in bats. <i>Cells Tissues Organs</i> 91, 272–282 (1975).
546	33.	K. Ito, V. T. Tu, T. P. Eiting, T. Nojiri, D. Koyabu, On the embryonic development of the
547		nasal turbinals and their homology in bats. <i>Front. Cell Dev. Biol.</i> <b>9</b> , 1–19 (2021).
548	34.	L. R. Yohe, <i>et al.</i> , Evaluating the performance of targeted sequence capture, RNA-Seq,
549		and degenerate-primer PCR cloning for sequencing the largest mammalian multigene
550		family. <i>Mol. Ecol. Resour.</i> <b>20</b> , 140–153 (2020).
551	35.	E. V. Koonin, Evolution of genome architecture. Int. J. Biochem. Cell Biol. 41, 298–306
552		(2009).
553	36.	Y. Niimura, M. Nei, Comparative evolutionary analysis of olfactory receptor gene
554		clusters between humans and mice. <i>Gene</i> <b>346</b> , 13–21 (2005).
555	37.	J. R. Arguello, <i>et al.</i> , Extensive local adaptation within the chemosensory system

556		following Drosophila melanogaster's global expansion. <i>Nat. Commun.</i> <b>7</b> , ncomms11855
557		(2016).
558 559	38.	H. B. Treloar, A. M. Miller, A. Ray, C. A. Greer, "Development of the Olfactory System" in <i>The Neurobiology of Olfaction</i> , 1st Ed., A. Menini, Ed. (CRC Press, 2010), pp. 131–155.
560	39.	J. H. Coleman, <i>et al.</i> , Spatial determination of neuronal diversification in the olfactory
561	57.	epithelium. <i>J. Neurosci.</i> <b>39</b> , 814–832 (2019).
562	40.	K. Mori, H. Von Campenhausen, Y. Yoshihara, Zonal organization of the mammalian
563		main and accessory olfactory systems. Philos. Trans. R. Soc. B Biol. Sci. 355, 1801–1812
564		(2000).
565	41.	S. Hayden, <i>et al.</i> , A cluster of olfactory receptor genes linked to frugivory in bats. <i>Mol.</i>
566		<i>Biol. Evol.</i> <b>31</b> , 917–27 (2014).
567	42.	L. R. Yohe, et al., Bayesian hierarchical models suggest oldest known plant-visiting bat
568		was omnivorous. <i>Biol. Lett.</i> <b>11</b> , 1–5 (2015).
569	43.	S. J. Hand, <i>et al.</i> , A new, large-bodied omnivorous bat (Noctilionoidea: Mystacinidae)
570		reveals lost morphological and ecological diversity since the Miocene in New Zealand.
571		<i>Sci. Rep.</i> <b>8</b> , 235 (2018).
572	44.	J. Camacho, et al., Peramorphosis, an evolutionary developmental mechanism in
573		neotropical bat skull diversity. <i>Dev. Dyn.</i> <b>248</b> , 1129–1143 (2019).
574	45.	K. T. J. Davies, <i>et al.</i> , Foraging shifts and visual preadaptation in ecologically diverse
575		bats. <i>Mol. Ecol.</i> <b>29</b> , 1839–1859 (2020).
576	46.	J. Potter, et al., Dietary diversification and specialization in Neotropical bats facilitated
577		by early molecular evolution. <i>Molecualar Biol. Evol.</i> (2021)
578		https:/doi.org/10.1093/molbev/msab028.
579	47.	L. R. Yohe, <i>et al.</i> , Tissue collection of bats for -omics analyses and primary cell culture.
580		<i>J. Vis. Exp. JoVE</i> <b>152</b> , e59505 (2019).
581	48.	J. Brechbühl, G. Luyet, F. Moine, I. Rodriguez, MC. Broillet, Imaging pheromone sensing
582		in a mouse vomeronasal acute tissue slice preparation. J. Vis. Exp. 58, e3311 (2011).
583	49.	M. D. MacManes, The Oyster River Protocol: a multi-assembler and kmer approach for
584		de novo transcriptome assembly. <i>PeerJ</i> <b>6</b> , e5428 (2018).
585	50.	R. Smith-Unna, C. Boursnell, R. Patro, J. M. Hibberd, S. Kelly, TransRate: Reference-free
586		quality assessment of de novo transcriptome assemblies. <i>Genome Res.</i> 26, 1134–1144
587		(2016).
588	51.	S. Hayden, <i>et al.</i> , Ecological adaptation determines functional mammalian olfactory
589		subgenomes. <i>Genome Res.</i> <b>20</b> , 1–9 (2010).
590	52.	E. Paradis, J. Claude, K. Strimmer, APE: analyses of phylogenetics and evolution in R
591		language. <i>Bioinformatics</i> <b>20</b> , 289–290 (2004).
592	53.,	VGstudio Max 3.3. <i>Vol. Graph. GmbH</i> (2014).
593	54.	M. a. Miller, W. Pfeiffer, T. Schwartz, Creating the CIPRES Science Gateway for inference
594		of large phylogenetic trees in <i>Proceedings of the Gateway Computing Environments</i>

595 596 Workshop (GCE), (leee, 2010), pp. 1-8.

# 597 Figures

598 **Figure 1**. Phylogeny of cumulative taxa used in this study. Iodine-stained µCT-scans were used 599 to reconstruct olfactory epithelium of different turbinates. RNA-seg of the main olfactory 600 epithelium was used to identify protein-coding sequences of expressed olfactory receptors. Animal-feeding taxa are highlighted in grey, as determined from the continuous values from 601 602 Rojas *et al.*, (2018). Numbers on the phylogeny correspond to species illustrations on the right. 603 Illustrations on the far right are medial sagittal sections of the nasal cavity of respective 604 species with the turbinate olfactory epithelium illustrated in separate colors. Illustrations were 605 done by Sara Scranton.

606

607 **Figure 2**. (A) Olfactory epithelium segmented from its distribution along the turbinate bones of two phyllostomid species. Artibeus boqotensis is an obligate frugivorous bat, while 608 609 *Gardnerycteris crenulatum* is a specialized insectivore. (B) Differences between main olfactory 610 epithelium and respiratory epithelium observed from the iodine-stained  $\mu$ CT-scans. This is 611 example is a transverse section in *Sturnira oporaphilum*. Panel (A) shows how olfactory 612 epithelium is present on the frontoturbinal and ethmoturbinal I, but more dorsal views of the 613 transverse section (lower panel) show that these turbinates are now covered in respiratory 614 epithelium. Skull image from Animal Diversity Web. Colors correspond to respective turbinate 615 bone shown in Figure 1. (C-D) Output from bayou of theta estimates of olfactory epithelium surface area trait evolution in branches with regime shifts with greater than (C) 0.25 posterior 616 617 probability and (D) 0.1 posterior probability. Colors correspond to branches from tree in figure 618 1 in which notable rate shifts occur. (E) Parameter estimates of MCMCqlmm, testing for a 619 relationship of olfactory epithelium surface area and body mass, explained by diet. Open circles 620 denote posterior estimates overlap with zero; grey circles denote 95% credible intervals 621 overlap with zero; and black circles indicate the entire posterior distribution is above or below 622 zero. Note that mormoopids were removed from the analyses in panel C. The only regime shift 623 with greater than 0.5 posterior probability included only mormoopids, shown in Figure S6, S7. 624

625 **Figure 3.** Branch length estimates of each *olfactory receptor (OR)* gene plotted as nucleotide rates versus codon model rates and colored by (A) diet and (B) OR subfamily. PCA axes of codon 626 627 and nucleotide branch lengths colored by (C) diet and (D) OR subfamily. Posterior distribution 628 parameter estimates (E) of hierarchical models testing for relationship of OR subfamily and 629 nucleotide branch lengths with codon branch length. Open circles denote posterior estimates 630 overlap with zero; grey circles denote 95% credible intervals overlap with zero; and black circles 631 indicate the entire posterior distribution is above or below zero. Arrows in panels B and D 632 correspond to higher or lower rates of evolution as shown in panel E.

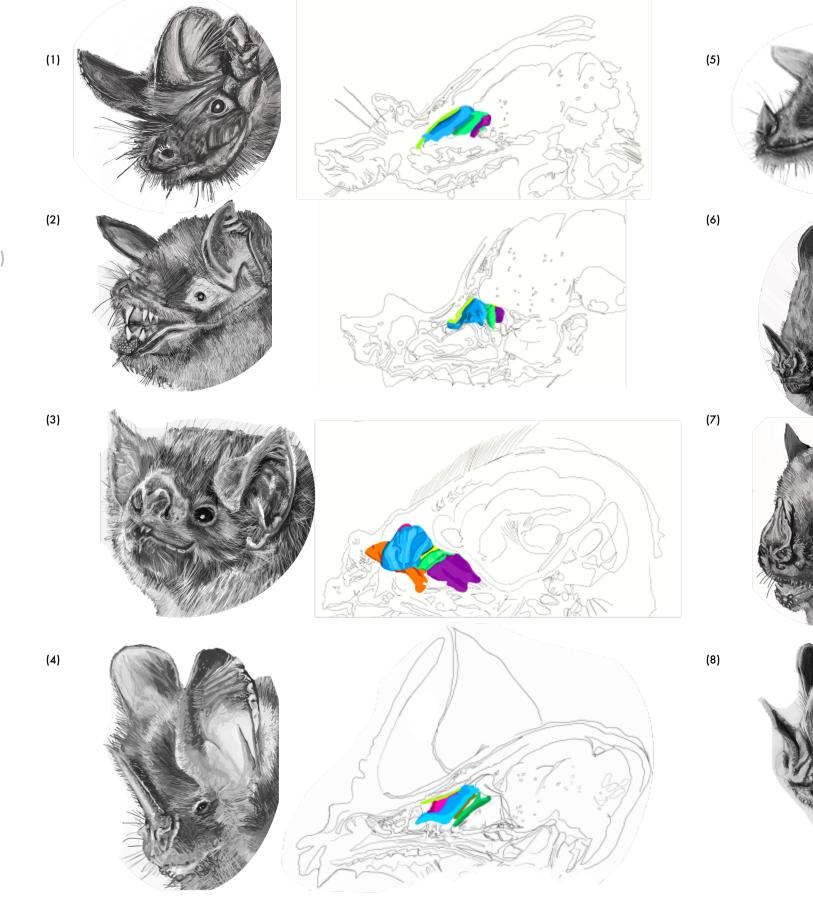
**Figure 4**. Posterior distributions of parameter estimates of hierarchical models from analyses 635 combining molecular and morphological data. (A) Estimated coefficients on codon branch 636 lengths and (B) estimated coefficients of covariates on olfactory epithelium surface area. Open 637 638 circles denote posterior estimates overlap with zero; grey circles denote 95% credible intervals overlap with zero; and black circles indicate the entire posterior distribution is above or below 639 zero. To interpret these plots, when a coefficient posterior is above zero, there is a positive 640 relationship with the response, and when it is below zero, there is a negative relationship with 641 642 the response. 643

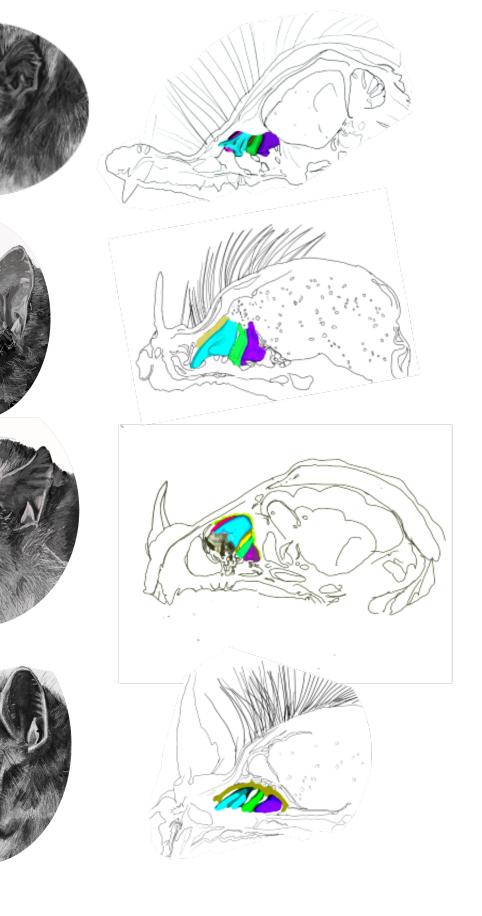
- Myotis albescens Tadarida brasiliensis (1) Molossus molossus Molossus rufus - Saccopteryx leptura Saccopteryx bilineata - Noctilio leporinus Mormoops blainvillei Pteronotus pusillus (2) Pteronotus quadridens - Macrotus waterhousii - Desmodus rotundus (3) — Tonatia saurophila - Gardnerycteris crenulatum (4) Phyllostomus elongatus – Phyllostomus hastatus - Anoura geoffroyi (5) · Monophyllus redmani Glossophaga soricina · Brachyphylla pumila Erophylla bombifrons - Phyllonycteris poeyi Lionycteris spurrelli – Carollia castanea r Carollia sowelli Carollia brevicauda <sup>L</sup> Carollia perspicillata – Rhinophylla pumilio · Rhinophylla fischerae (6) – Sturnira parvidens L Sturnira oporaphilum (7) — Uroderma bilobatum · Chiroderma villosum Vampyrodes caraccioli Mesophylla macconnelli Vampyressa thyone Phyllops falcatus • Artibeus bogotensis (8) - Artibeus fraterculus • Artibeus planirostris <sup>L</sup> Artibeus jamaicensis 40 20

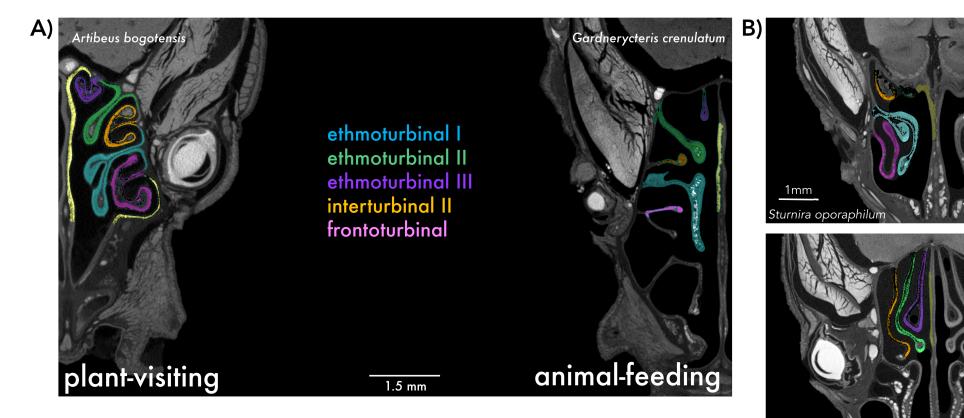
residual olfactory epithelium
 ethmoturbinal I
 interturbinal
 ethmoturbinal II
 frontoturbinal II
 interturbinal II

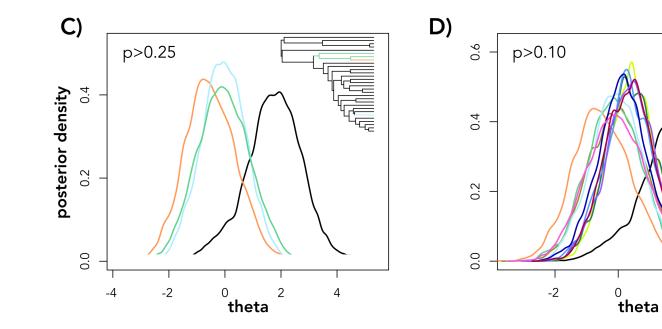
60

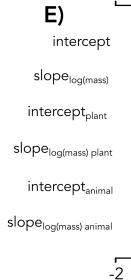
Ma











Sturnira opora

